Available online at www.sciencedirect.com
SCIENCE DIRECT®
Applied Catalysis A: General 263 (2004) 91–101
APPLIED CATALYSIS A: GENERAL
www.elsevier.com/locate/apcata

Raman studies of Rh and Pt on La_2O_3 catalysts used in a membrane reactor for hydrogen production

L.M. Cornaglia*, J. Múnera, S. Irusta, E.A. Lombardo

Instituto de Investigaciones en Catálisis y Petroquímica, (FIQ, UNL-CONICET), Santiago del Estero 2829-3000 Santa Fe, Argentina

Received in revised form 2 December 2003; accepted 2 December 2003

Abstract

Rh and Pt catalysts supported on lanthanum oxide were prepared by wet impregnation. The solids were used in a Pd–Ag membrane reactor to produce hydrogen through the carbon dioxide reforming of methane. The effect of the sweep gas flow rate and W/F upon the conversions of CO_2 and CH_4, as well as on the production of H_2 was studied. The best performing catalyst was Rh (0.6%). It yielded a methane conversion 38% higher than the thermodynamic value and the highest H_2 permeate flux across the membrane. Lanthanum phases on the support and the catalysts were characterized by Laser Raman spectroscopy, FTIR, and XRD. The support and the calcined fresh catalysts exhibited a mixture of phases which were influenced by the metal type. Furthermore, platinum seemed to favor the formation of Ia-$La_2O_2CO_3$ after a short treatment in flowing CO_2. However, the only remaining crystalline phase after 100 h on stream was II-$La_2O_2CO_3$. A small amount of graphitic carbon was detected using Laser Raman spectroscopy, despite the fact that no carbon deposition was observed through TGA measurements. The graphite crystallization order seemed to be dependent upon the contact time of the reactants.

Keywords: Membrane reactor; Dry reforming; Raman spectroscopy; Lanthanum; Carbon deposits

1. Introduction

The process of methane reforming with carbon dioxide could contribute to reduce the amount of greenhouse gases present in the atmosphere. Besides, hydrogen is extensively used by the oil industry in hydrotreating and hydro-cracking processes, and also in fuel cell applications [1]. During the past ten years, the CH_4 dry reforming reaction has received considerable attention, and efforts have been focused on the development of catalysts showing high activity and resistance to coking. Numerous supported metal catalysts have been tested for this process. Among them, noble metal [2–5] containing solids give promising catalytic performance in terms of methane conversion and selectivity to synthesis gas.

Membrane reactors (MR) might have a very important role in the development of new processes with high energetic efficiency. Several hydrogenation–dehydrogenation reactions were studied in Pd-based MRs [6,7]. A membrane reactor offers the possibility to achieve methane conversions greater than thermodynamic values [8,9].

Lanthanum oxide has found numerous applications in catalysis. It is recognized as an active, selective catalyst for several processes [10,11]. It is well known that the composition and activity of La_2O_3 for methane oxidative coupling is highly dependent on the preparation and activation procedure used [12]. Lanthanum oxide is also used as support for metals that catalyze reactions such as methanol decomposition [13], ammonia oxidation [14], and methane dry reforming [15]. It has also been shown that lanthana oxides can substantially modify the chemical behavior of highly dispersed metal catalysts [16].

In the lanthanum oxide system, several chemical species can be present such as La_2O_3, $La(OH)_3$, $La_2(CO_3)_3$, and $La_2O_2(CO_3)$. There are three polymorphic crystalline forms of $La_2O_2(CO_3)$. All are layer-type structures built up of slabs of $(La_2O_2{}^{2+})_n$ polymers and $CO_3{}^{2-}$ groups. Type-I has the square $(La_2O_2{}^{2+})_n$ layers found in LnOCl and related compounds (tetragonal), while type-II has the hexagonal $(La_2O_2{}^{2+})_n$ layers found in the A-form sesquioxides. Type-Ia, on the other hand, has monoclinic form [17]. The

* Corresponding author. Tel.: +54-3424536861; fax: +54-3424536861.
E-mail address: lmcornag@fiqus.unl.edu.ar (L.M. Cornaglia).

0926-860X/$ – see front matter © 2003 Elsevier B.V. All rights reserved.
doi:10.1016/j.apcata.2003.12.003

presence of certain phases (e.g. oxycarbonates) has been connected with the catalytic stabilities of lanthanum oxide supported Ni solids.

Raman spectroscopy has been employed to characterize lanthanum compounds such as La_2O_3, $La(OH)_3$ [18–20]; however, scarce data are found related to the different types of lanthanum oxycarbonates.

Besides, carbon compounds have particularly large Raman scattering cross sections, which has been used in materials science to monitor the properties of carbon. Despite these advantages, however, it has not been much used for measurements of catalytic carbon deposits [15,21,22].

The present paper reports on the use of laser Raman spectroscopy, FTIR, XRD to characterize the Rh and Pt catalysts supported on lanthanum oxide before and after being used for carbon dioxide reforming in a membrane reactor.

2. Experimental

2.1. Catalyst preparation

Catalysts were prepared by the conventional wet impregnation of La_2O_3 (Anedra 99.99%) using $H_2(PtCl_6)\cdot 6H_2O$ and $RhCl_3\cdot 3H_2O$ as precursor compounds. The pH of impregnation solution was 3. In all cases, the resulting suspension was then heated at 353 K to evaporate the water, and the solid material was dried in an oven at 383 K overnight. The catalysts were calcined for 6 h at 823 K. In experiments designed to investigate the effect of carbon dioxide in the absence of CH_4, the catalysts were heated at 773 K for 1 h, and cooled down in flowing CO_2 using a flow reactor before taking the IR and Raman spectra.

The Rh and Pt dispersions, following the H_2 reduction at 823 K for 2 h, was determined by hydrogen desorption experiments [9]. The dispersions were 64, 14, and 17% for Rh (0.2%), Rh (0.6%), and Pt (0.93%) catalysts, respectively.

To prepare II-$La_2O_2CO_3$, La_2O_3 (Anedra) was heated under flowing dry CO_2 using a temperature program consisting of a linear 5 K min^{-1} ramp from 300 to 923 K, a linear 2 K min^{-1} ramp from 923 to 973 K, and finally an isothermal heating at 973 K for 30 min [12]. Preparation of Ia-$La_2O_2CO_3$ was performed by thermally decomposing La_2O_3 (Aldrich 99.99% Gold Label). The oxide was heated at 10 K min^{-1} from 298 to 773 K under flowing He. The flow was then switched to dry CO_2 and the temperature kept at 773 K for 1 h.

2.2. Catalyst testing

The double tubular membrane reactor was built using a commercial dense Pd–Ag alloy (inner tube), provided by REB Research and Consulting, with one end closed and an inner tube to allow helium sweep gas flow. The outer tube was made of commercial non-porous quartz (i.d. 9 mm). The catalyst, diluted with quartz chips to achieve a bed height of 3 cm, was packed in the outer annular region (shell side). The inner side of the membrane in all runs was kept at atmospheric pressure. The catalysts were heated in He at 823 K and then reduced in situ in H_2 at the same temperature for 2 h. After reduction, the feed stream gas mixture (33% CH_4 v/v, 33% CO_2, 34% He, $P = 1.013$ bar) was switched through the reactor.

In order to measure the equilibrium conversions, the membrane reactor was operated with no sweep gas and no pressure difference between the tube and the shell sides. In this case, the conversions were measured after a 12 h stabilization period.

The reaction products and the permeated mixture were analyzed with a TCD gas chromatograph equipped with a Porapak and a molecular sieve column and with an on-line Balzers Quadstar TU 422 quadrupole mass spectrometer previously calibrated for each gas. The carbon balance was close to one in all cases.

2.3. X-ray diffraction (XRD)

The XRD patterns of the calcined and used solids were obtained with an XD-D1 Shimadzu instrument, using Cu Kα radiation at 35 kV and 40 mA. The scan rate was 1 ° min^{-1} for values between $2\theta = 10^\circ$ and 80°.

2.4. FT infrared

The IR spectra were obtained using a Shimadzu FTIR 8101 M spectrometer with a spectral resolution of 4 cm^{-1}. The solid samples were prepared in the form of pressed wafers (ca. 2 wt.% sample in KBr).

2.5. Laser Raman spectroscopy (LRS)

The Raman spectra were recorded with a TRS-600-SZ-P Jasco Laser Raman instrument, equipped with a CCD (charge coupled device) with the detector cooled to about 153 K using liquid N_2. The excitation source was the 514.5 nm line of a Spectra 9000 Photometrics Ar ion laser. The laser power was set at 30 mW. The spectral resolution was 4 cm^{-1}.

3. Results

3.1. Membrane reactor data

Fig. 1 compares the effect of the sweep gas upon both the conversion of the reactants and the mols of H_2 permeated through the membrane per mol of CH_4 fed. These data are given for Rh (0.2%) and Rh (0.6%), metal loading is shown between brackets. Increasing the He sweep gas flow rate reduces the hydrogen partial pressure in the permeate side leading to higher H_2 flow rate through the

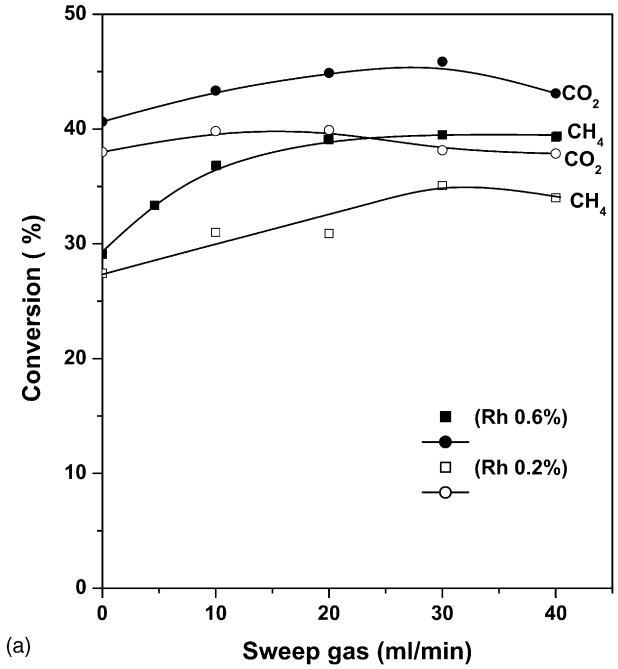

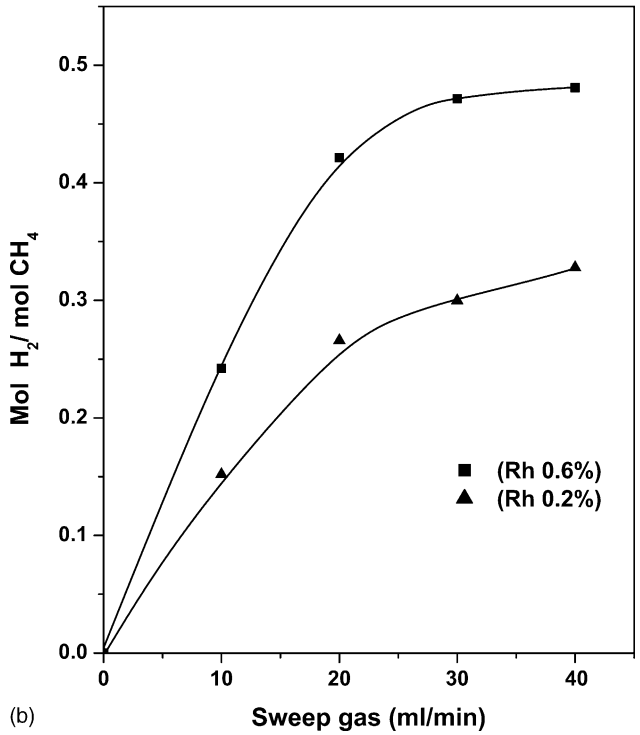

Fig. 1. Comparison of the effect of the sweep gas on the catalytic behavior of Rh (0.2%) and Rh (0.6%) solids: (a) CH_4 and CO_2 conversions; (b) hydrogen flux through the membrane. $T = 823\,K$, $W/F = 1.5 \times 10^{-3}\,g\,h\,ml^{-1}$, $\Delta P = 0$ bar.

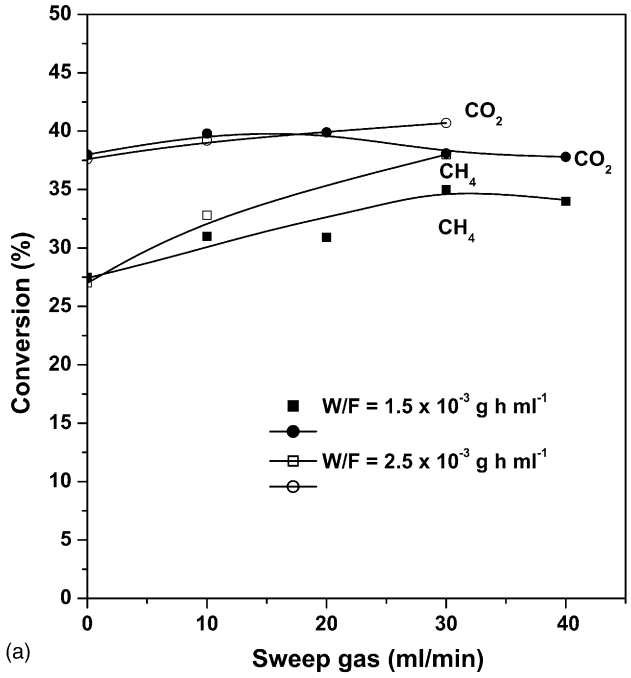

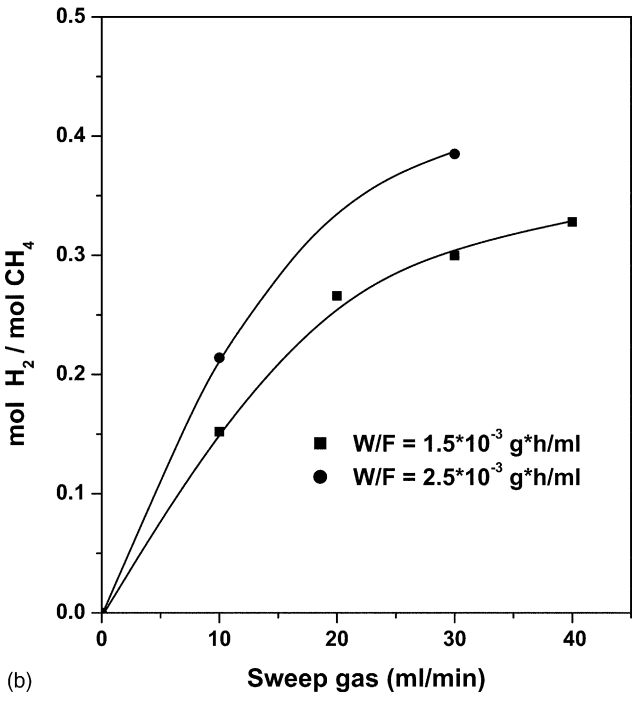

Fig. 2. Effect of the sweep gas and W/F on the catalytic behavior of Rh (0.2%) solid: (a) CH_4 and CO_2 conversions; (b) hydrogen flux through the membrane. $T = 823\,K$, $\Delta P = 0$ bar.

membrane (Fig. 1b). The increase in the metal loading causes an improvement of more than 4% in the methane and carbon dioxide conversions (Fig. 1a) and 0.16, the mol H_2 permeate/CH_4 ratio.

Fig. 2 shows the effect of the W/F on the catalytic behavior of the Rh (0.2%) catalyst. Note that in the presence of the catalyst, the reverse water gas shift reaction (RWGSR) proceeds very fast. This is why the CO_2 is always higher than the CH_4 conversion. However, in Fig. 2a it is seen that the difference between the conversions decreases as the H_2 (permeated)/CH_4 ratio increases (Fig. 2b). This could be explained in terms of the reduced H_2 pressure in the reaction side that would decrease the conversion of the RWGSR.

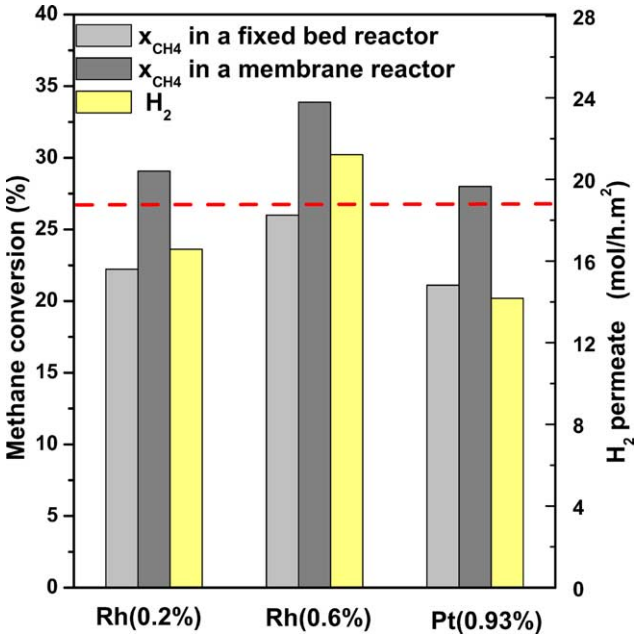

Fig. 3. Comparison of the methane conversion and the hydrogen flux on the Rh and Pt catalysts at $W/F = 5 \times 10^4$ g h ml^{-1}. $T = 823$ K. The dotted line indicates the thermodynamic value considering the dry reforming and the reverse WGSR.

Fig. 3 compares the three catalysts studied at $W/F = 5 \times 10^{-4}$ g h ml^{-1} and at 823 K with no sweep gas (fixed-bed reactor) and with a sweep gas flow rate of 10 ml min^{-1}. In all cases, the methane conversion achieved in the membrane reactor is above the equilibrium value.

The Rh catalysts showed stable conversions during 100 h on stream at $W/F = 1.5 \times 10^{-3}$ g h ml^{-1} and 823 K. However, the Pt (0.93%) solid showed decreased conversion after 24 h on stream under the same conditions. These results agree with those obtained using a fixed-bed reactor, which were previously reported [9,15].

3.2. X-ray diffraction data

Table 1 summarizes the lanthanum phases detected in the studied solids. The XRD pattern of the Aldrich support indicates that $La(OH)_3$ was the only phase present in this solid. On the other hand, the reflections of the solid treated with carbon dioxide at 773 K (not shown) reveal the major peaks of the monoclinic Ia-$La_2O_2CO_3$. Traces of type-II are also present.

Three phases, $La(OH)_3$, type-I and type-II $La_2O_2CO_3$, are identified in the Anedra support. After treating this solid in a flow of dry CO_2 at 973 K, the hexagonal (type II) phase becomes dominant. Only tiny signals of types I or Ia appear in this solid.

The XRD patterns for all the prepared catalysts showed the presence of II-$La_2O_2CO_3$ and $La(OH)_3$ phases (Table 1). La_2O_3 signals were also detected on the Pt (0.93%) catalyst. The XRD data of the used catalysts indicated that type-II was present, independent of both the metal type and loading.

No XRD reflections associated with Rh or Pt compounds were detected in the calcined catalysts. On the other hand, the XRD data of used Pt (0.93%) indicated the presence of

Table 1
Structural features of fresh and used catalysts and the support

Solids	DRX phases (ASTM number)	FTIR wavenumbers of CO_3^{2-} vibration (cm^{-1})			
		ν_3	ν_1	ν_2	ν_4
Rh (0.2%) calcined	II-$La_2O_2CO_3$ (37-804) $La(OH)_3$ (6-585)	1504(sh) 1467 1370	1087	856	747
Rh (0.6%) calcined	II-$La_2O_2CO_3$ (37-804) $La(OH)_3$ (6-585)	1504(sh) 1467 1370	1087	856	747
Rh (0.2%) and Rh (0.6%) used catalyst	II-$La_2O_2CO_3$ (37-804)	1508 1465	1087	856	747
Pt (0.93%)%) calcined	II-$La_2O_2CO_3$ (37-804) $La(OH)_3$ (36-1481) La_2O_3 (22-641)	1495 1465 1370(sh)	1087	856	747
Pt(0.93%)%) used catalyst	II-$La_2O_2CO_3$ (37-804) $La(OH)_3$ (36-1481) Pt^0	1508 1465	1087	856	747
Anedra support	II-$La_2O_2CO_3$ (37-804) $La(OH)_3$ (6-585)	1504(s) 1467 1370(s)	1087	856	747
Aldrich support	$La(OH)_3$ (6-585) $La(OH)_3$ (36-1481)	1462 1384		855	

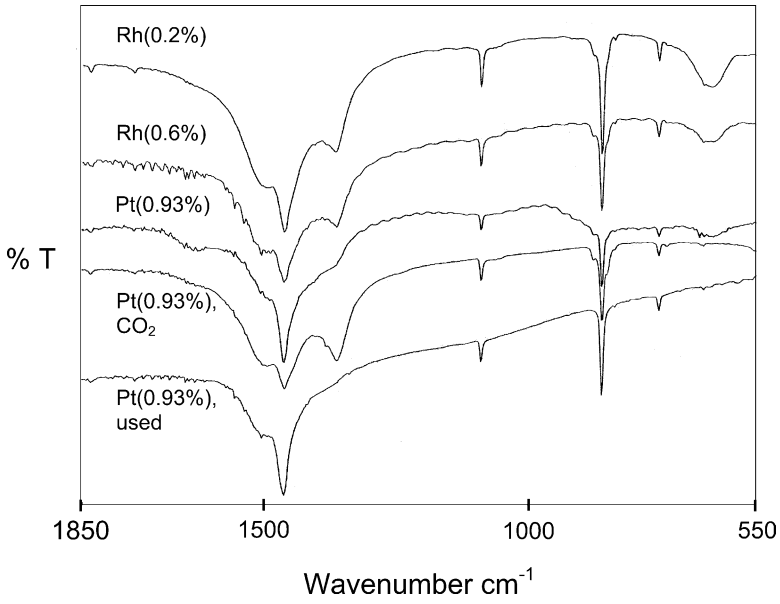

Fig. 4. FTIR spectra of rhodium and platinum supported catalysts, calcined, used and after CO_2 treatment at 773 K.

metallic platinum [9], while no metal signals where detected in used rhodium solids.

3.3. FT infrared results

The FTIR spectra of the calcined catalysts are presented in Fig. 4. The spectra of low metal loading catalysts show bands at 1504 (s), 1467, 1087, 856, and 747 cm^{-1} coincident with those of the hexagonal (type-II) structure of $La_2O_2CO_3$ [23]. In addition, a signal at 1368 cm^{-1} hints the presence of either the monoclinic (type-Ia) or the tetragonal (type-I) polymorph in Rh (0.2%) and Rh (0.6%) catalysts (Fig. 4). However, some slight splitting of these bands indicates the presence of the Ia polimorph. On the other hand, the Pt catalyst spectrum shows only a shoulder at 1368 cm^{-1} (Fig. 4). A broad band at 643 cm^{-1} corresponding to the OH bending vibration [24] is observed in all the spectra. The IR spectrum of Anedra support (not shown) exhibits the same phases as that of the Pt solid.

Fig. 4 shows the spectra of the catalysts after treatment in flowing CO_2. The shoulder at 1364 cm^{-1} grows in an intense band while signals in the 2800–2900 cm^{-1} region (not shown) almost vanish. This would indicate the development of type-I or Ia-$La_2O_2CO_3$ and the disappearance of carbonates (2800–2900 cm^{-1} bands) [25]. The splitting observed in the oxycarbonate bands indicates the presence of the Ia polimorph. On the other hand, the bands of rhodium-based catalysts did not show any change after treating the solid with CO_2. The FTIR spectrum of the used Pt (0.93%) (Fig. 4) is characteristic of the hexagonal phase (type-II). Spectra of used rhodium solids also correspond to the same phase. In both the used and the CO_2 treated catalysts, the OH vibration disappears.

3.4. Raman data

3.4.1. The support

Prior to studying the supported Rh and Pt catalysts, Raman spectra were taken of the pure reference phases and support materials. The structure of these materials was confirmed by XRD and FTIR [26]. The Raman spectra for the 250–800 cm^{-1} region are shown in Fig. 5a. The spectrum of lanthanum hydroxide exhibits four bands at 274, 339, 447, and 597 cm^{-1}. The frequencies of these bands are in agreement with those reported for crystalline $La(OH)_3$ [19].

No Raman data have been found in the literature for lanthanum oxycarbonates. The Raman spectrum of type-II-$La_2O_2CO_3$ shows three peaks in the 250–800 cm^{-1} region, at 358, 384, and 747 cm^{-1}. Besides, a strong band at 1086 cm^{-1} and weak ones at 1408, 1415, and 1450 cm^{-1} are seen (Fig. 5b).

The spectra of sodium and strontium carbonates are taken as references. In both cases a strong peak at 1070 cm^{-1} and a weak peak at 1430 cm^{-1} were detected. The $La_2(CO)_3$ shows a band at 1066 cm^{-1} [19]. Taking into account the lower Raman shift for carbonates and the wavenumber of the ν_1 CO_3^- vibration in the FTIR spectra, the strong band at 1086 cm^{-1} can be assigned to lanthanum oxycarbonate. The presence of the carbonate group was confirmed by the bands recorded at the 1400–1450 cm^{-1} region (see Table 2).

Type-Ia-$La_2O_2CO_3$ spectrum presents several overlapping peaks at 294, 315, 338, 356, 387, and 437(sh), 450 cm^{-1}. Multiple splitting is observed in the 700–1500 cm^{-1} region (Fig. 5b). The strongest band appears at 1060 cm^{-1}. The IR characteristic band at 1373 cm^{-1} is observed at 1340 cm^{-1} in the Raman spectrum.

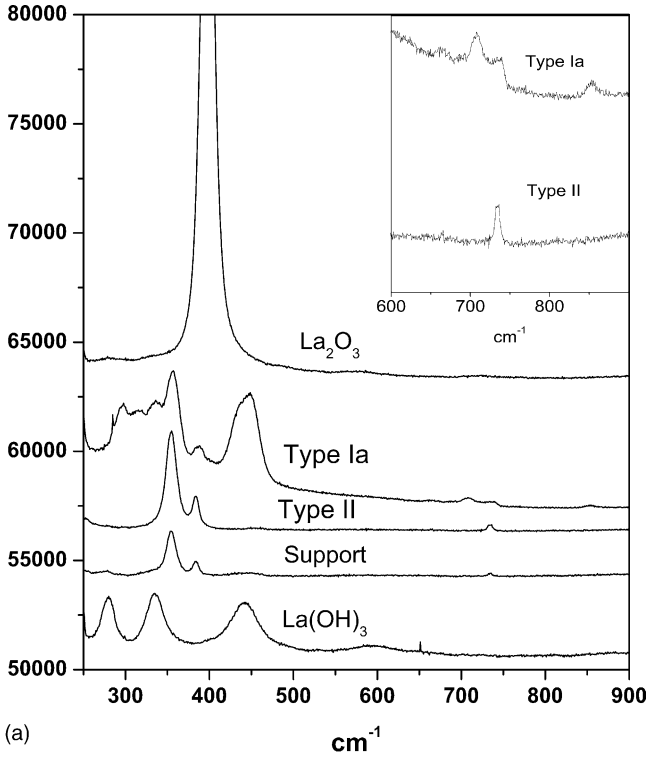

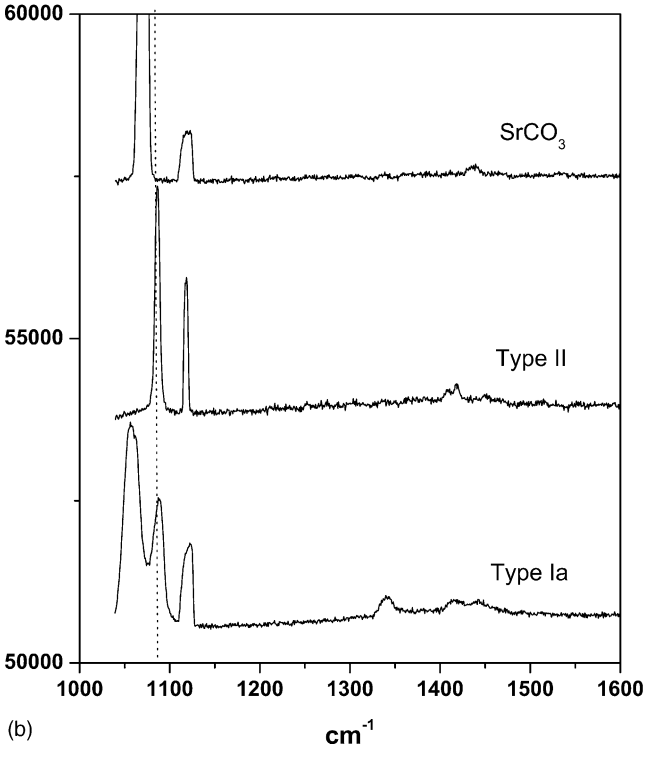

Fig. 5. Laser Raman spectra of reference phases: (a) 250–900 cm^{-1} region; (b) 1000–1600 cm^{-1} region.

The spectrum of the support (Anedra) calcined at 823 K indicates that the main phase is II-$La_2O_2CO_3$. Besides, the weak bands at 284, 342, and 452 cm^{-1} reveal the presence of small amounts of $La(OH)_3$.

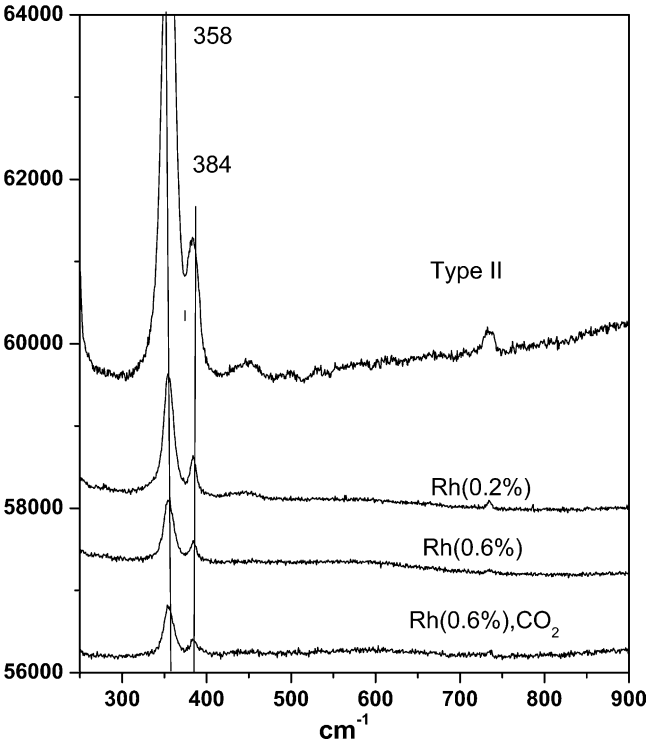

Fig. 6. Laser Raman spectra of Rh catalysts calcined and after CO_2 treatment at 773 K.

3.4.2. Calcined catalysts

The spectra of the Rh catalysts are shown in Fig. 6. All the solids treated at 823 K exhibit peaks at 358, 384, 747, and 1086 cm^{-1} (not shown) assigned to the type-II lanthanum oxycarbonate.

In the case of the platinum catalyst (Fig. 7), the spectrum is similar to those recorded for the Rh solids, with weak bands at 426 and 443 cm^{-1}. These features correspond to type-Ia oxycarbonate. After treatment with CO_2, the former bands became well defined.

3.4.3. Used catalysts

Raman spectroscopy is an effective method to study properties of the different carbon materials [27–29], including catalytic carbon, carbon nanotubes, carbonaceous particles, carbon films, and synthetic diamond. The Raman spectra of the various form of graphite have been discussed extensively in the literature [30]. The first order transitions lie between 1200 and 1700 cm^{-1}.

Fig. 8 shows the Raman spectra of different samples of carbon deposits formed on Rh and Pt catalysts. All the spectra have a group of similar bands at 1339 (D mode), 1593 (G mode) with a shoulder at 1612 (D′ mode). The graphitic nature of carbon deposits can be deduced from the observation of the G and D bands.

The band at 1593 named the G peak is the E_{2g} mode of bulk graphite; its intensity scales with the crystal size. The band at 1620 was assigned to the analogue of the E_{2g} mode for the graphite layers located at the boundary of the

Table 2
Raman shift of catalysts and lanthanum compounds

Solid	250–700 (cm^{-1} region)	CO_3^- 700–1500 (cm^{-1} region)			
Rh (0.6%) calcined	358, 384	–	1087	–	747
Rh (0.2%) calcined	358, 384	1408, 1415, 1450	1087	–	747
Rh (0.2%) used catalyst	358, 384	1408, 1415, 1450	1087	–	747
Pt (0.93%)	358, 384, 426, 443	1408, 1415, 1450	1087	–	747
Pt (0.93%) used catalyst	358, 384	–	1087	–	747
II-$La_2O_2CO_3$	358, 384	1408, 1415, 1450	1087	–	747
Ia-$La_2O_2CO_3$	294, 315, 340, 356, 387, 437(sh), 450	1340, 1417, 1444	1057, 1089	852	707, 737
$La(OH)_3$	284, 339, 447, 597	–	–	–	–
La_2O_3	400	–	–	–	–

crystals and was designated E'_{2g} or D′. It is sensitive to the composition of the material in contact with the surface layers of the graphite, which modifies their electronic environment.

The feature near 1340 cm^{-1}, designated the D (disorder) band is allowed only if the $k = 0$ selection rule breaks down and this occurs near the crystal edges. Wang et al. [31] have suggested that this band originates in the edge vibrations since its frequency is independent of chemical composition or sample preparation.

In Fig. 8 it can be seen that the D is more intense than the G band for all the carbonaceous species formed in the three types of catalysts used in the membrane reactor and evaluated at several space velocities. The spectra are normalized against the support band at 1086 cm^{-1}. The small signals appearing at ca. 1400 cm^{-1} are due to the oxycarbonates.

The spectra were fitted using the model applied by Sze et al. [32] for carbonaceous aerosols. For the fitting procedures, they specified Lorentzian lineshapes at the frequencies of the D, G, and D′ transitions and allow these to vary slightly, within the resolution of the spectrometer (4 cm^{-1}). The fitted spectra of the Rh (0.6%) solid after 180 h on stream in the membrane reactor is shown in Fig. 9. The results of spectra fitting for all catalysts are summarized in Table 3.

In Table 3, the data for commercial graphite and both the Ni and Ni–Rh/La_2O_3 catalysts are included. These catalysts contained large amounts of carbon after being used in a fixed-bed reactor at temperatures between 823 and 973 K. The dry reforming reaction [15] was always under equilibrium conditions in these experiments.

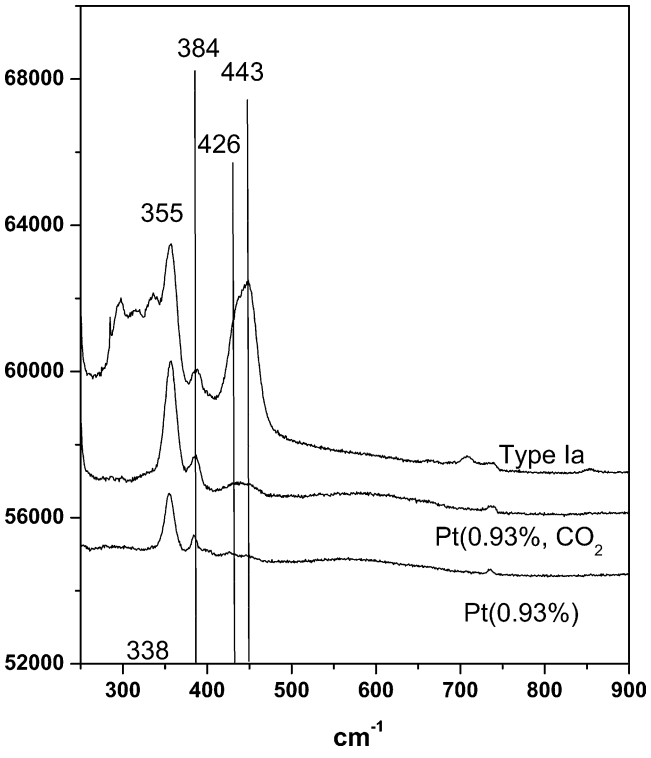

Fig. 7. Laser Raman spectra of Pt catalyst calcined and after CO_2 treatment at 773 K.

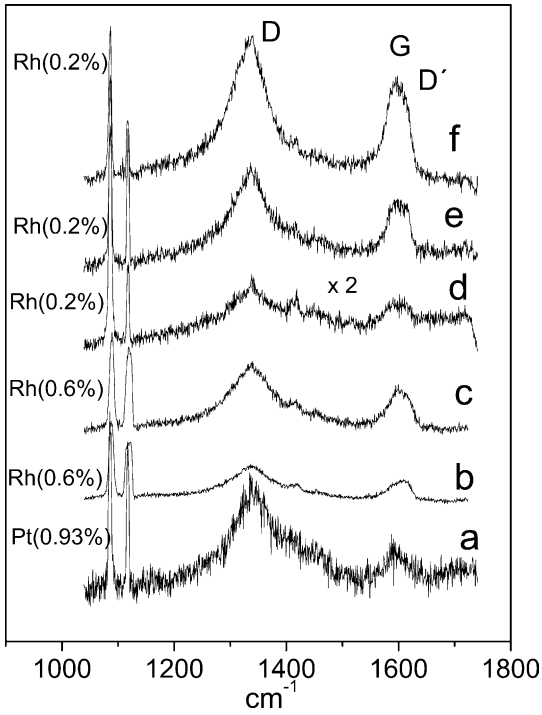

Fig. 8. Laser Raman spectra of Rh and Pt catalysts used in the membrane reactor at different W/F: (a) 3.2×10^{-3} g h ml^{-1}; (b) 1.5×10^{-3} g h ml^{-1}; (c) 2.5×10^{-3} g h ml^{-1}; (d) 5.0×10^{-4} g h ml^{-1}; (e) 1.5×10^{-3} g h ml^{-1}; (f) 2.5×10^{-3} g h ml^{-1}.

Table 3
Raman data for used catalysts in the membrane reactor

Catalysts[a]	W/F	ID/IG	LA (nm)	D′/G	$I_{1086}/I_{1336+1590}$
Ni (2%)[b]	7.3×10^{-5}	1.4	2.8	0.18	0.03
Ni (2%) Rh (0.2%)[b]	7.3×10^{-5}	1.6	3.1	0.16	0
Rh (0.2%)	2.5×10^{-3}	3.3	1.5	0.2	0.06
	1.5×10^{-3}	4.6	1.2	0.33	0.10
	0.5×10^{-3}	6.3	0.70	0.30	0.30
Rh (0.6%)	2.5×10^{-3}	4.4	1.2	0.20	0.09
	1.5×10^{-3}	6.6	1.0	0.46	0.18
Pt (0.93%)	3.2×10^{-3}	11.2	0.73	0	0.07

[a] Graphite ID/IG = 0.39, LA = 11 nm, G = 1565 cm^{-1}, D = 1337 cm^{-1}.
[b] Catalystic test: fixed-bed reactor, temperature range 823–973 K. Reaction time: 48 h. From Irusta et al. [15].

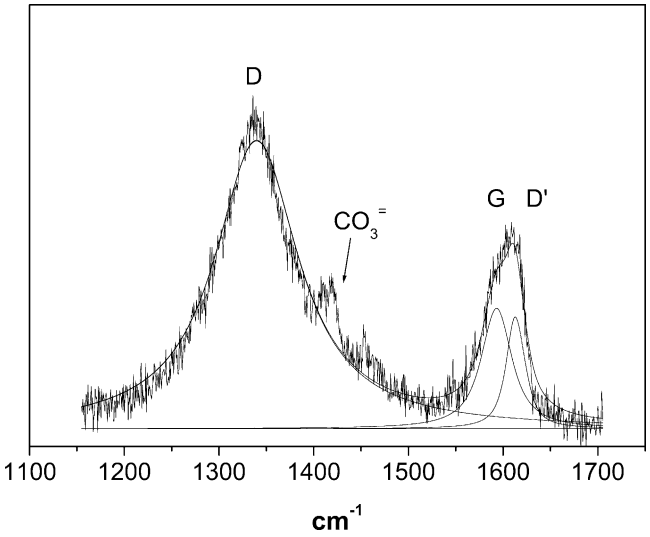

Fig. 9. Laser Raman spectrum of Rh (0.6%) solid after 180 h on stream fitted using Lorentzian curves located at the frequencies of the D, G, and D′ bands.

The position of the D band remains essentially constant for all the samples. However, the G band appears at 1565 cm^{-1} for graphite, 1560 cm^{-1} for the Ni catalysts, and 1592 cm^{-1} for the Rh and Pt containing solids. This 30 cm^{-1} shift is coincident with the presence of disordered carbon in these solids.

4. Discussion

4.1. Catalytic performance in the membrane reactor

In agreement with the data reported by other groups for the same reaction using different solids [8,9,33], conversions above equilibrium can be achieved with the three catalysts (Fig. 3).

The difference in hydrogen partial pressure across the membrane is the driving force for the permeation of this gas. When the sweep gas flow rate increases, the permeation should do the same. Increasing the He flow rate, the hydrogen partial pressure in the permeate side decreases leading to higher permeation flow rate (Fig. 1).

In a fixed bed reactor the RWGSR occurs together with the dry reforming of methane. In the membrane reactor, part of the hydrogen produced is withdrawn from the reaction side and since this is one of the reactants for the RWGSR, the conversion of CO_2 should decrease accordingly. This could explain the decrease in CO_2 conversion observed for both Rh catalysts (Fig. 1a).

The reverse water gas shift reaction could be avoided if we used a membrane giving a higher rate of H_2 permeation than that of H_2 formation. Kikuchi [33] using Pt/Al_2O_3 stabilized with basic compounds reported that hydrogen formation on those catalysts was slower than hydrogen permeation, so that the RWGS reaction was not important in the Pd–Ag membrane reactor. However, they observed deactivation after a short time on stream (8 h).

Liu and Au [34] using a La_2NiO_4 zeolite membrane reactor observed that CH_4 and CO_2 conversions were significantly higher than those recorded over a commom fixed-bed reactor. Ferreira-Aparicio et al. [35] employed mesoporous ceramic filters in a membrane reactor to carry out the reforming of methane with carbon dioxide. By increasing the sweep gas flow rate, changes in the gas composition were observed at both sides of the membrane. These variations led to moderate conversion enhancements. However, membranes with high permeability but low selectivity for hydrogen also cause reactants to be removed from the reaction side, limiting the conversion increase.

The different values of the methane and carbon dioxide conversions obtained in our membrane reactor suggested that hydrogen formation was always higher than hydrogen permeation. The use of a highly selective membrane which could allow a higher permeation flow rate would improve the performance of the membrane reactor.

Fig. 3 compares the three catalysts assayed at a given W/F without sweep gas and with 10 ml min^{-1} of sweep gas. The data obtained without sweep gas are identical to those obtained using a fixed-bed reactor [9]. Note that in this case the TOFs decrease in the direction: Rh(0.6%) > Rh(0.2%) > Pt(0.93%). Furthermore, the Pt catalyst deactivates with time on stream. In all cases the methane

conversion is higher than the thermodynamic value. The best performing catalyst, Rh (0.6%), yields a methane conversion 38% higher than the thermodynamic value together with the highest H_2 permeate flux across the membrane.

4.2. Catalysts characterization

4.2.1. The support

A variety of compounds may develop when lanthanum oxide is exposed to different gas mixtures. The composition of the resulting solids depends on the preparation method and the pretreatment. This system is very sensitive to the presence of water vapor and CO_2 in the gas phase [36]. In the literature FTIR, XRD, and to a lesser extent Laser Raman spectroscopy, have been used to characterize the lanthanum compounds. The information obtained from the LRS complements that obtained from FTIR and XRD, and allows a more detailed understanding of the catalyst structure.

The oxycarbonate Raman spectra show bands in the 250–450 cm^{-1} region (Table 2). These bands can be assigned to the La–O fundamental modes. Besides, the bands in the 700–1500 cm^{-1} region correspond to the ν_1, ν_2, ν_3, and ν_4 vibration of CO_3^- groups by comparison with the FTIR results [26].

Type-II oxycarbonate is characterized by strong Raman bands at 358, 384, and 1087 cm^{-1}. In the case of type-Ia oxycarbonate, the Raman spectrum is more complicated, in agreement with the infrared data discussed by Turcotte et al. [17] and Irusta et al. [26]. Type-Ia IR spectrum shows a threefold splitting of the ν_1, ν_2, and ν_3 modes and multiple splitting of the ν_4 mode. The Raman spectrum clearly exhibited the threefold splitting of the ν_3 mode and multiple splitting of the ν_1 and ν_4 modes.

4.2.2. The catalysts

Lanthanum supported metal catalysts are often prepared by impregnation of the oxide with aqueous solutions of the metal precursor salt. Since La_2O_3 is highly reactive in the presence of water, a strong chemical and structural rearrangements of the support would occur. As a result of the intense carbonation phenomena induced on lanthana by the impregnation process, the actual nature of the support phases would depend on the impregnation method and the treatments of the impregnated samples [36].

Calcined catalysts with low rhodium loading (0.2 and 0.6%) show an increase in type-Ia polymorph (Fig. 4) that was already present in the support. Ni (2%)/La_2O_3 solid (not shown) also revealed an increase in Ia-$La_2O_2CO_3$. However, the Raman results indicate a different behavior. The Rh (0.6%) Raman spectrum only reveals the presence of type-II oxycarbonate. Platinum, on the other hand, would not modify the phases of the lanthanum oxide (Figs. 4, 5 and 7).

Verykios and coworkers [37,38] found a strong interaction between carbon dioxide and the support in Ni/La_2O_3 catalysts. This led to the formation of $La_2O_2CO_3$ species, detected by XRD and FTIR which would react with carbon deposited onto Ni particles at the interface between Ni and oxycarbonate, thus offering an active and stable performance. After ca. 0.5 h of reaction, type-Ia and type-II oxycarbonates were formed. The proportion of these phases only changed slightly up to 100 h on stream [37]. No formation of $La_2O_2CO_3$ was observed by Slagtern et al. [39] on the La–Ni–Al–O catalysts. Oxycarbonates may nevertheless be outside the detection limit of the method used, and they did not reach any conclusion about their role in the deactivation process. On Co and Ni La-based catalysts prepared from perovskite precursors [40] the La_2O_3 phase that existed in the reduced catalysts disappeared after 3 h on stream. Instead, type-Ia and type-II-$La_2O_2CO_3$ phases were formed due to the adsorption of CO_2 on lanthanum oxide. These authors claimed that oxycarbonate may play a crucial role in the CO_2 reforming of CH_4. Identification of those lanthanum compounds is mainly based on DRX and FTIR since no Raman data have been reported for these cartalysts. All our solids exposed to the reaction atmosphere only presented II-$La_2O_2CO_3$ (Fig. 4), while the monoclinic (type-Ia) phase present in the calcined catalysts disappeared. The Raman data of the used catalysts (not shown) confirm these observations. Since the Rh catalysts are very stable, it seems that II-$La_2O_2CO_3$ plays an important role in maintaining the high performance of these solids.

The CO_2 treated catalysts yielded more information about the interaction of this reactant with the solids. Pt (0.93%) exposed to CO_2 shows a significant enhancement in the presence of Ia-$La_2O_2CO_3$ (Figs. 4, 6 and 7), while the lanthanum phases present in the Rh solids were not affected by this treatment. One possible explanation for this significant difference in reactivity arises from the strong Rh–La interaction reported for these catalysts [15]. The formation of a thin surface layer of $LaRhO_3$ could impair the phase transformation. Calculations based on the lattice constants of the perovskite [41] show that for Rh (0.2%) and Rh (0.6%) solids 50 and 100% of the support surface could be covered by a monolayer of rhodate, respectively. An alternative explanation could be that Pt catalyzes type-Ia oxycarbonate formation by reaction of the support with CO_2 while Rh does not promote this gas–solid interaction. The experimental data obtained so far do not provide conclusive evidence for any of these options.

4.3. Carbon characterization

Different types of deactivating coke deposits have been reported for methane reforming on metal catalysts such as adsorbed atomic carbon, amorphous carbon, bulk carbide, and crystalline graphitic carbon [4,15]. In Ni/La_2O_3 catalysts [37], the layers of lanthanum carbonate could hinder the formation of deactivating coke, possibly by limiting the formation of an encapsulating veil around the Ni particle. In the case of rhodium supported on other oxides, a low sensitivity to coking has been previously reported. Solymosi and coworkers [42,43] proposed that CH_x fragments formed in

the decomposition of methane reacted with CO_2, thus impairing their complete decomposition to surface carbon.

For all the used catalysts reported in the present paper, no carbon deposition was observed through TGA measurements [9]. However, a small amount of graphitic carbon was detected using Laser Raman spectroscopy.

In view of the band assignments, it seems clear that the relative intensities of these features can be used to retrieve information about the sizes and morphologies of the graphite crystals. In the case of hexagonal crystal graphite, the Raman spectra consists of the main first order band (G band) assigned to the in plane displacement of carbon atoms in the hexagonal sheets. When disorder is introduced into the graphite structure the existing bands broaden and additional bands are found at about 1350 cm^{-1} (D mode) and 1620 cm^{-1} (D′ mode). In the rather small or disordered crystal with very little three dimensional order, the G and D′ bands merge into a single broader feature. The G peak indicates the presence of large graphite crystals, while the ratio of the D to G peaks gives the relative amount of edge to volume of the crystals.

The integral intensity ratio ID/IG is inversely proportional [44] to the microcrystalline planar size (LA), which corresponds to the in plane dimension of single microcrystalline domains in graphite. The D and G modes were also found to be sensitive to the type of carbon bonding, i.e. sp^2 and sp^3 hybridization. It has recently been shown [44] that the relationship below holds for a wide array of sp^2-bonded carbons over the range $2.5 < LA < 300$ nm for laser wavelenghts of 488 and 514.4 nm.

$$\frac{ID}{IG} = \frac{4.4\,nm}{LA}$$

The values in the fourth column of Table 3 were obtained employing the previous formula. Based on the data in Table 3, the samples can be classified into different types by the ordering of the graphite structures formed. The first group presents the highest disordering of graphite structure. The ID/IG intensity ratio is greater than 3.3. The average crystallite size is estimated by the formula to be less than 1.5 nm. In this case, the literature reports some divergence between the crystal size estimated by XRD and the one predicted by the formula. Reshetenko et al. [44] noted that Raman spectroscopy is more sensitive than XRD to reveal the intrinsic defects of graphite lattice. The amount of amorphous phase can be estimated from the intensity of the band at 1336 cm^{-1}.

The second group of solids is characterized by the intermediate defectiveness of the graphite structure. The ID/IG intensity ratios are 1.6 and 1.4 (Ni (2%), Rh (0.2%)) and the average crystallites sizes are 2.8 and 3.1 nm, respectively. The ID/IG ratio is 0.39 (<1) for commercial graphite with crystallite sizes of 11 nm.

In the Rh catalysts the D/G relative intensity is higher for the solids tested at lower W/F ratios. This result seems to indicate that the crystallization order is a function of the contact time (space velocity). Furthermore, it is clearly seen that the solids evaluated at higher W/F (near the thermodynamic equilibrium) exhibit higher intensity bands due to larger amounts of graphitic carbon being formed. Note that all the catalysts have been exposed to similar amounts of reactants during 180 h on stream. Comparing the spectrum of the Pt catalyst (a) with the one obtained for Rh (0.6%) (c) it is concluded that the latter contains a lower proportion of disordered carbon.

In Rh and Pt–La-based catalysts, the carbon deposits did not affect the activity after 100 h in the membrane reactor. This behavior could be related to the sites on which carbon is deposited and/or to the role that carbon would play as a reaction intermediate.

5. Conclusions

- For all the catalysts the methane and carbon dioxide conversions obtained in the membrane reactor are higher than the thermodynamic values. The Rh (0.6%) solid yields the highest permeated hydrogen/fed methane ratio.
- The support and the calcined fresh catalysts exhibit a mixture of phases. The latter are being influenced by the metal type. Furthermore, platinum seems to favor the formation of Ia-$La_2O_2CO_3$ after a short treatment in flowing CO_2.
- It is clear from these studies that independent of the phases initially present in these catalysts, after 190 h on stream at 823 K, the only remaining crystalline phase is II-$La_2O_2CO_3$.
- A small amount of graphitic carbon was detected using Laser Raman spectroscopy, despite the fact that no carbon deposition was observed through TGA measurements.
- The Raman data suggests that the graphite crystallization order was dependent upon the contact time of the reactants. The carbon species formed on the Pt catalyst exhibits a lower crystallization order.

Acknowledgements

The authors wish to acknowledge the financial support received from UNL, CONICET, and ANPCyT. They are also grateful to the Japan International Cooperation Agency (JICA) for the donation of the major instruments used in this study. Thanks are finally given to Prof. Elsa Grimaldi for the edition of the English paper.

References

[1] L. Paturzo, F. Galluci, A. Basile, G. Vitulli, P. Pertici, Catal. Today 82 (2003) 57.
[2] S. Irusta, L. Cornaglia, E. Lombardo, J. Catal. 210 (2002) 263.
[3] L. Wang, K. Murata, M. Inaba, Catal. Comm. 4 (2003) 147.
[4] M. Bradford, M. Vannice, Catal. Rev. Sci. Eng. 41 (1999) 1.

[5] L. Mattos, E. Rodino, D. Resasco, F. Passos, F. Noroña, Fuel Process. Tech. 83 (2003) 147.
[6] L. Van Dyk, S. Miachon, L. lorenzen, M. Torres, K. Fiaty, J.-A. Dalmon, Catal. Today 82 (2003) 167.
[7] G. Marigliano, G. Barbieri, E. Drioli, Chem. Eng. Process. 42 (2003) 231.
[8] A.K. Prabhu, R. Radhakrishnan, S. Ted Oyama, Appl. Catal. A: Gen. 183 (1999) 241.
[9] J. Múnera, S. Irusta, L. Cornaglia, E. Lombardo, Appl. Catal. A: Gen. 245 (2003) 383.
[10] S.J. Huang, A.B. Walters, M.A. Vannice, J. Catal. 192 (15) (2000) 29.
[11] M. Traykova, N. Davidova, J.-S. Tsaih, A.H. Weiss, Appl. Catal. A: Gen. 169 (2) (1998) 237.
[12] R. Taylor, G. Schrader, Ind. Eng. Chem. Res. 30 (1991) 1016.
[13] G. Mul, A.S. Hirschon, Catal. Today 65 (1) (2001) 69.
[14] J. Petryk, E. Kowakowska, Appl. Catal. B: Environ. 24 (2) (2000) 121.
[15] S. Irusta, L. Cornaglia, E. Lombardo, J. Catal. 210 (2002) 7.
[16] H. Vidal, S. Bernal, R. Baker, G. Cifredo, D. Finol, J. Rodríquez-Izquierdo, Appl. Catal. A: Gen. 208 (2001) 111.
[17] R. Turcotte, J. Sawyer, L. Eyring, Inorg. Chem. 8 (1969) 238.
[18] M. Scheithaeur, H. Knözinger, H.M. Vannice, J. Catal. 178 (1998) 701.
[19] S. Chan, A. Bell, J. Catal. 89 (1984) 433.
[20] D.L. Hoang, A. Dittmar, M. Schneider, A. Trunschke, H. Lieske, K. Brzezinka, K. Witka, Thermochim. Acta 400 (2003) 153.
[21] H. Hayashi, M. Kishida, K. Wakabayashi, Catal. Survey Jpn. 6 (2002) 9.
[22] S. Liu, G. Xiong, H. Dong, W. Yang, Appl. Catal. A: Gen. 202 (2002) 141.
[23] J. Moggia, V. Milt, M. Ulla, L. Cornaglia, Surf. Interface Anal. 35 (2003) 216.
[24] T. Le Van, M. Che, J.M. Tatibouet, M. Kermarec, J. Catal. 142 (1993) 18.
[25] B. Klingenberg, A. Vannice, Chem. Mater. 8 (1996) 2755.
[26] S. Irusta, L. Cornaglia, E. Lombardo, Mater. Chem. Phys., submitted for publication.
[27] C. Klinke, R. Kurt, J.M. Bonard, K. Kern, J. Phys. Chem. B 106 (2002) 1191.
[28] R. Escribano, J.J. Sloan, N. Siddique, N. Sze, T. Dudev, Vib. Spectrosc. 26 (2001) 179.
[29] L. Cornaglia, A. Gellman, J. Vac. Sci. Technol. 15 (1997) 2755.
[30] F. Tuinstra, J.L. Koening, J. Chem. Phys. 53 (1970) 1126.
[31] Y. Wang, D.C. Alsemeyer, R. Mc Creery, Chem. Mater. 2 (1990) 557.
[32] S. Sze, N. Siddique, J. Sloan, R. Escribano, Atm. Environ. 35 (2001) 561.
[33] E. Kikuchi, Catal. Today 25 (1995) 333.
[34] B.S. Liu, C.T. Au, Catal. Lett. 77 (2001) 67.
[35] P. Ferreira-Aparicio, I. Rodríguez-Ramos, A. Guerrero-Ruiz, Appl. Catal. A: Gen. 237 (2002) 239.
[36] S. Bernal, F. Botana, R. García, F. Ramírez, J. Rodríguez-Izquierdo, Appl. Catal. 31 (1987) 267.
[37] Z. Zhang, X. Verykios, Appl. Catal. A.: Gen. 138 (1996) 109.
[38] X. Verykios, Int. J. Hydrogen Energy 28 (2003) 1045.
[39] A. Slagtern, U. Olsbye, R. Bom, I. Dahl, H. Fjellvåg, Appl. Catal. A: Gen. 165 (1997) 379.
[40] J. Guo, H. Luo, Y. Zhu, X. Zheng, Mater. Lett. 57 (2003) 4450.
[41] L. Chonghe, T. Yihao, Z. Yingzhi, W. Chunmei, W. Ping, J. Phys. Chem. Solids 64 (2003) 2147.
[42] J. Raskó, F. Solymosi, Catal. Lett. 46 (1997) 153.
[43] A. Erdöhelyi, J. Cserényi, F. Solymosi, J. Catal. 141 (1993) 287.
[44] T. Reshetenko, L. Avdeeva, Z. Ismagilov, V. Pushkarev, S. Cherepanova, A. Chuvilin, V. Likholobov, Carbon 41 (2003) 1605.